An Exploratory Aerodynamic Limits Test with Analytical Correlation

Matthew W. Floros Nili Peretz Gold
Raytheon ITSS
Moffett Field, California

Wayne Johnson
Army/NASA Rotorcraft Division
NASA Ames Research Center
Moffett Field, California

The purpose of the current test program is to produce a new dataset with sufficient documentation to be useful for correlation, development, and refinement of aerodynamic models at high thrust. An aerodynamic limits test was conducted in the 7- by 10-Foot Wind Tunnel at Ames Research Center. The objectives of the test were to measure the performance and control loads of the rotor in nominal thrust, lightly stalled, and deep stalled conditions. Advance ratios from 0.15 to 0.35 were tested with data concentrated at an advance ratio of 0.2. Shaft angle was varied from 0 to -2 deg with tip speeds of 310 and 446 ft/sec. Thrust and power measurements were found to be high quality and repeatable at different rotor speeds and shaft angles. Redundant torsion load information recorded with two strain gages on the pitch horns and a gage on the blade showed that the pitch horn gages were consistent while the blade torsion measurement was not. CAMRAD II predictions of thrust and power correlated well with the test data.

Notation

A	rotor disk area
D	rotor drag
C_H	rotor inplane force coefficient
C_{P_i}	induced power coefficient
C_{P_o}	profile power coefficient
C_{P_P}	propulsive power coefficient
EA	Blade section tensile stiffness
EI_{FLAP}	flapwise blade section stiffness
EI_{LAG}	chordwise blade section stiffness
GJ	Blade torsion stiffness
I_θ	blade section torsional moment of inertia
I_P	blade section polar moment of inertia
P_i	induced power
P_o	profile power
P_P	propulsive power
Q	rotor torque
R	rotor radius
T	rotor thrust
V	tunnel speed
V_T	rotor tip speed
W_M	weight on metric side of balance
X	rotor longitudinal inplane drag/propulsive force (wind axes)
X_{cg}	chordwise location of blade section center of gravity
X_t	rotor longitudinal inplane force tare
X_{tc}	chordwise location of blade section tension center
c_{d_0}	airfoil drag at zero lift
d	rotor diameter
q	tunnel dynamic pressure
Ω	rotor speed
α_s	rotor shaft angle
μ	advance ratio
ρ	air density
σ	rotor solidity
ψ	rotor azimuth angle

Introduction

One of the most important characteristics of a helicopter rotor is its maximum thrust. The amount of thrust a rotor can generate determines the rotor size and maneuvering limits for the aircraft. A number of rotor components are sized based on stresses encountered near the thrust limit, particularly in maneuvers where the rotor is beginning to stall. Despite this, accurate methods to predict rotor performance as it enters stall remain elusive.

Static stall determines the limits on maximum thrust and the power required. Dynamic stall contributes to large control system and rotor component loads that govern aircraft load limits. In dynamic stall, a vortex is shed from the leading edge. As it passes over the airfoil chord, there are unsteady increments in lift and drag but more importantly a large variation in pitching moment. This pitching moment

may determine the size of components in the control system, hub, and blades.

A number of dynamic stall models have been developed over the past two decades with several in common usage today (Refs. 1–3). Models have often been compared with 2-D airfoil data and in some cases with flight test data (Ref. 4). There are a number of comparisons of stall models with 2-D data, but few comparing to 3-D data, i.e. wind tunnel or flight test. For model validation and development, wind tunnel data are preferable due to the tighter control on operating condition and flow quality and the relative absence of aerodynamic interactions.

A model scale CH-47B/C rotor at high speed and thrust was tested by McHugh *et al.* in the late 1970's (Refs. 5–7). The goals were to identify the extremes of speed and thrust that were possible with a conventional rotor producing thrust and propulsive force, and to measure the performance and control loads near those extremes. The blades were built with sufficient strength that the aerodynamic limits could be reached before the structural limits. Data were acquired for attached flow, light stall, and deep stall. For many cases, a hard aerodynamic limit was observed, where the rotor would stall sufficiently that total thrust would decrease with increasing collective pitch.

The data were recently re-examined by Yeo (Ref. 8) and correlated with the comprehensive analysis CAMRAD II and flight test data from the UH-60 Airloads Program (Ref. 9) to determine their suitability for correlation work. Reynolds number corrections were applied to match the full scale and model scale data and a variety of dynamic stall models were compared. Inspection of refs. 5 and 6 revealed differences in repeat runs of the same test conditions which could not be explained. Also, the data were found to be of limited utility because documentation of the blade properties and the blades themselves no longer exist.

The Aeroflightdynamics Directorate, US Army Aviation and Missile Research, Development and Engineering Center, initiated the current test program in order to produce a new dataset with sufficient documentation to be useful for correlation, development, and refinement of aerodynamic models at high thrust. The test entry described in this paper was an exploratory test to provide scope for a more involved test in the future. Data from the current test are compared with data from the McHugh test and the UH-60A Airloads Program and calculations from CAMRAD II.

Hardware and Instrumentation

A 2-bladed NACA 0012 rotor was tested in the 7- by 10-Foot Wind Tunnel at Ames Research Center. It was mounted on the US Army Rotary Wing Test Stand (RWTS) with a teetering hub and the US Army VSB-54 rotor balance. An installation photo is shown in Figure 1.

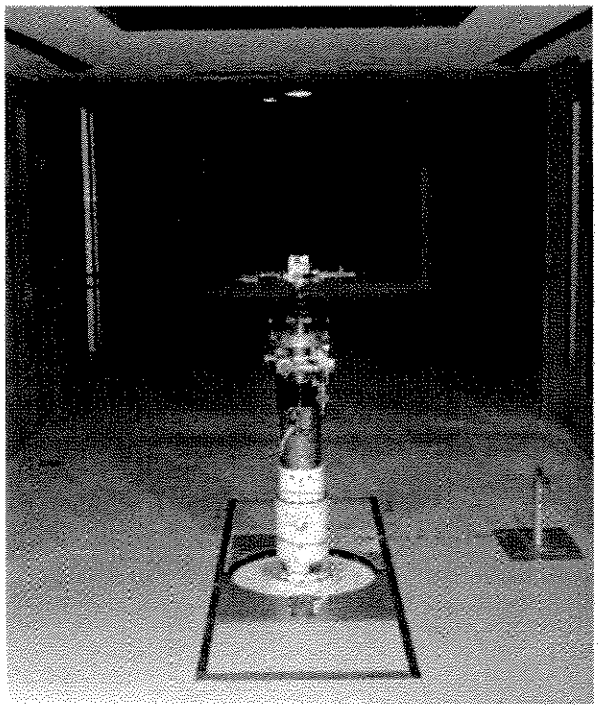

Fig. 1. Installation photo of US Army RWTS stand and teetering hub in 7- by 10-Foot Wind Tunnel.

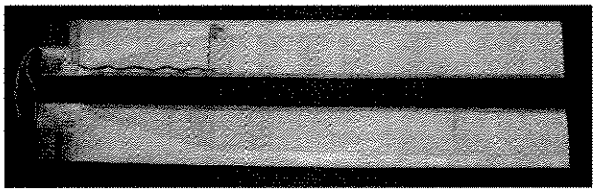

Fig. 2. NACA 0012 blades used in test.

The untwisted blades are constructed with a tapered aluminum spar, balsa wood filler, and a spruce trailing edge. A fiberglass skin provides a smooth aerodynamic surface, protects the shape and moisture content of the balsa, and adds some stiffness, particularly in lag, to the blade. The rotor properties are given in Table 1. Detailed discussion of the stiffness properties is provided with the description of the analytical model. A photograph of the blades is shown in Figure 2.

The primary instrumentation for the test was the balance, the blade instrumentation, and pitch horn instrumentation. Specifically, the balance measured five components of the rotor forces in the fixed frame and a flexible coupling measured the rotor torque. The blade instrumentation was used to monitor loads for safety of flight as well as provide engineering data. The strain gages on the blade were

Table 1. Properties of blades and rotor used in aerodynamic limits test

Radius, R	3.437 ft
Length (blade only)	2.968 ft
Chord	4 in (constant)
Airfoil	NACA 0012
Twist	none
Root attachment	RWTS teetering hub
Solidity, σ	0.06192
Precone, β_p	$1°20'$
Undersling, Z_{us}	0.03 ft
Rotation	Clockwise
δ_3	0

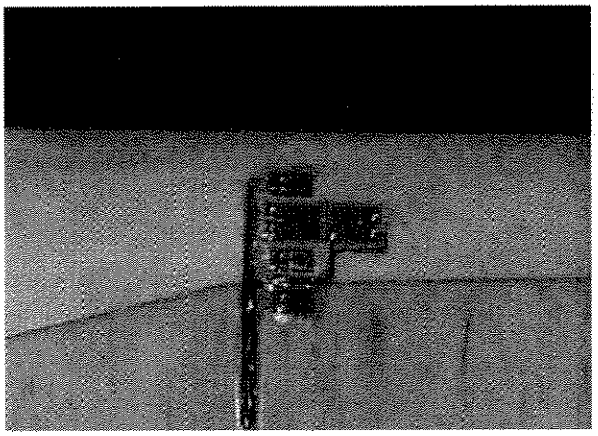

Fig. 3. Flap, lag, and Torsion strain gage (lower surface of blade) at maximum load point, approximately 0.42R.

bonded to the fiberglass skin, not to the wood or aluminum spar. Only one of the two blades was instrumented.

Flap, lag, and torsion were measured using strain gages at approximately $0.42R$. The taper of the spar resulted in the highest stresses occurring at this point. The spar is visible through the fiberglass in Figures 2 and 3. The cluster of blade instrumentation is also shown in Figure 3. Only the lower side is shown, but the flapping moment bridge was completed with a gage on the opposite side of the blade.

Redundant torsion measurements were acquired using a strain gage rosette on the blade and a strain gage on each of the pitch horns. The pitch horns were instrumented rather than the pitch links themselves for better sensitivity. The high axial stiffness of the pitch links would limit the precision of the data. The pitch horn measurements were calibrated as a root torsion moment on the blade. The blade and pitch link load measurements were intended to measure the same quantity.

Approximately 56 revolutions were averaged to obtain the steady forces, and vibratory loads were extracted from the 1024/rev time history data. All data acquired were synchronized with the rotor using a 1024/rev and 1/rev encoder. The encoder triggered a sample of data to be collected. Measurements were acquired in groups of 8 channels, with a $3\mu s$ delay between each channel, so up to a $21\mu s$ discrepancy can exist between two given measurements. This is negligible compared to the rotor speed, corresponding to about 0.15 deg azimuth at 1220 RPM.

Test Conditions

Aerodynamic limits data were acquired by performing collective sweeps at fixed shaft angle and advance ratio for two different rotor speeds. Figure 4 shows the matrix of conditions tested. For each point, the rotor was trimmed to zero flapping. At each condition, the collective pitch was increased until a load limit was reached on the rotor, balance, or test stand.

The blades were tested at low rotor speeds, 860 and 1220 RPM (310 and 446 ft/sec tip speeds), so that the aerodynamic limits could be attained before the structural limits of the blades and balance were reached. The 860 RPM condition represents half of the tip speed of the McHugh data in refs. 5 and 6. At this rotor speed, the oscillatory inplane balance limits were nearly reached as the rotor entered stall. In deep stall, although the blade loads continued to increase, the fixed-system balance loads were reduced. Maximum thrust was then limited by oscillatory blade flap or lag bending loads.

In a subsequent test, several changes to the test equipment would provide more comprehensive data. Because the thrust was limited in part by large steady flapping moments, an articulated rotor might have been a better choice for a high thrust test. Flap and/or lag hinges would relieve the steady moments and might reduce oscillatory moments on the blade as well. Also, a higher capacity balance would allow higher oscillatory inplane loads to be tolerated, although measurement sensitivity might be reduced.

1220 RPM represents twice the dynamic pressure in hover ($1220^2/860^2 \approx 2$) or about 75% of the dynamic pressure of the McHugh test. At 1220 RPM, the rotor could begin to stall within balance limits, but the maximum thrust was limited to only a lightly stalled condition by inplane loads on the balance. At rotor speeds higher than 1220 RPM, the oscillatory fixed system loads exceeded the balance limits before rotor stall occurred.

In contrast to the McHugh data, which focused on both high speed and thrust, the primary flight condition for the current investigation represents a maneuvering flight condition, at an advance ratio of $\mu = 0.2$. Data are concentrated at this speed although data were acquired over the range of $0.15 \leq \mu \leq 0.35$. No wall corrections were applied to the data for the results shown in this paper.

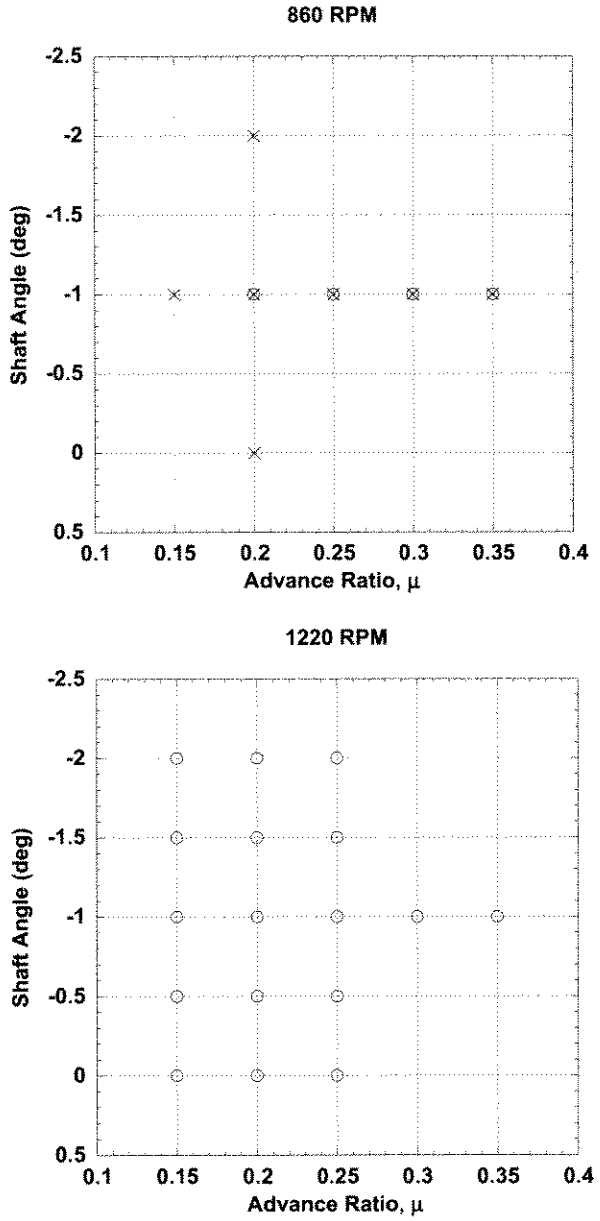

Fig. 4. Graphical depiction of flight conditions tested at 860 and 1220 RPM. Several repeat points were taken at 860 RPM, indicated by different symbols.

Another difference from the McHugh data was in the trim condition. For the McHugh test, the rotor was trimmed to a fixed propulsive force $X/(qd^2\sigma)$ and shaft angle was adjusted to maintain the propulsive force as collective increased. During the current test, the rotor was held at a fixed shaft angle for each sweep of collective. This allowed for better repeatability of the data because the force measurements were not being used real time to trim the flight condition. Also, by fixing shaft angle, the rotor could be tested at lower collective pitch settings. If propulsive force were fixed, then in low thrust conditions, the rotor would have to be tilted to large angles to generate the specified propulsive force.

The shaft angles ranged from $-2.0 \leq \alpha_s \leq 0$ deg. The data are concentrated near a condition of $\alpha_s = -1.0$ deg, $\mu = 0.2$. This represents a propulsive force coefficient of $X/(qd^2\sigma) \approx 0.05$ at a nominal thrust coefficient C_T/σ of 0.08. For a rotor with thrust parallel to the shaft, the precise angle of -0.92 deg corresponds to $X/(qd^2\sigma)$ of 0.05 at $C_T/\sigma = 0.08$. This angle was rounded to -1 deg since the test objective was not to replicate the McHugh data exactly. At each shaft angle, the collective pitch was increased until a load limit was reached on the blades or balance.

Data Reduction

Tares were not taken during the test entry. In order to correct for aerodynamic drag of the hub and weight of components on the metric side of the balance, tares had to be estimated from other information.

To estimate the drag tare, a combination of measurements and empirical estimates was used. Although blade-off tares were not recorded, five test points were recorded with the rotor at zero thrust, zero shaft angle, and zero flapping. In this condition, the rotor is only producing drag.

The test points were taken at 1220 RPM in 0.05 increments in advance ratio over the range $0.15 \leq \mu \leq 0.35$. These five points indicate the variation of drag with velocity for the rotor with blades on. The points were measured at a single RPM, but the tare was required for both 860 RPM and 1220 RPM. Therefore, the tare was curve-fitted with dimensional velocity rather than advance ratio so it could be used for different rotor speeds.

To obtain the drag of the blades themselves, an empirical expression for inplane force with advance ratio (Ref. 10) was used,

$$C_H = \frac{\sigma c_{d_0}}{8}(3\mu + 1.98\mu^{2.7}) \qquad (1)$$

Having measured the drag of the blades and hub and calculated the drag of the blades only, the hub drag was estimated by subtracting the two. Any (presumably small) differences in hub drag with shaft angle were not accounted for.

Once the aerodynamic tare was calculated, the final tare to be accounted for was that due to gravity. Although the maximum shaft angle tested was 2 deg, the large weight of the components above the balance show a significant effect on the inplane forces even when multiplied by the sine of a small angle. The gravity tare was taken from a previous test (Ref. 11) using the same rotor stand, balance, and hub, and similar blades. By curve-fitting the gravity tare to a sine function, a weight W_M of approximately 172 lb was obtained for all hardware on the metric side of the balance. This weight was included in the balance zero for thrust, so the only potential correction would be a cosine effect of the shaft angle. At the maximum shaft angle tested, a 172 lb vertical load on the balance is reduced by about 0.1 lb. Such a small correction could have been neglected, but was included in the data reduction for consistency with the inplane correction.

The weight of the blades themselves was approximately 4.5 lb, so they were a minor contributor to the 172 lb gravity tare. Thus differences in the weight between the current blades and those in the previous test should also be negligible.

The total longitudinal force tare in terms of V, μ, and α_s was then given by

$$X_t = 0.912 + 0.00703V + 0.00101V^2 - \frac{\sigma c_{d_0}}{8}(3\mu + 1.98\mu^{2.7})\rho A V_T^2 + W_M \sin\alpha_S \quad (2)$$

Rotor drag was calculated as

$$X = X_{\text{measured}} - X_t \quad (3)$$

This tare was found to adequately collapse the data at a given advance ratio.

Test Data

The objective of the test was to measure thrust, torque, and pitch link loads as the rotor enters stall. The performance and loads data are presented in the following sections.

Performance Data

To present the performance data, the propulsive component of power was removed. In flight, the propulsive force opposes the vehicle drag and is dependent on the drag of the fuselage. For the wind tunnel test, the propulsive power is produced by the rotor shaft being tilted as the rotor is trimmed to zero flapping. By removing it, the remaining power is that required to produce the rotor lift (induced power) and to rotate the blades (profile power). The profile plus induced power is obtained by subtracting the propulsive power from the total,

$$P_o + P_i = Q\Omega - P_P \quad (4)$$

where the propulsive power P_P and its non-dimensional coefficient C_{P_P} are given by

$$P_P = -XV \quad (5)$$

$$C_{P_P} = \frac{P_P}{\rho A V_T^3} \quad (6)$$

The thrust is plotted vs. power in Figures 5–9 for advance ratios from 0.15 to 0.35. The limitations of the blade and balance loads are evident from the extent of the data. In Figure 5, lowest advance ratio, the maximum C_T/σ achieved is 0.146 for the 860 RPM condition, but only about 0.105 for 1220 RPM. At the highest advance ratio, Figure 9, the maximum C_T/σ have been reduced to the 0.07–0.08 range for both rotor speeds. At 1220 RPM, at every advance ratio, the rotor was just entering stall (identified by the change in the lift curve slope) when the load limits were reached. The 860 RPM runs extended into stall except for the highest advance ratio case.

Note that a maximum thrust, after which a thrust reversal occurs, is not present in any of the results. A slope change is evident, indicating stall, but the thrust continues to increase post-stall. The character of the stall changes as advance ratio increases. In Figures 5 and 6, the lift curve slope change is fairly abrupt at C_T/σ of 0.1. At the higher advance ratios, the lift curve slope is already decreased at C_T/σ of 0.1, but a discrete point is difficult to see.

Propulsive force is plotted vs. thrust in Figures 10–14. X is positive aft, so propulsive force is negative when the rotor is supplying propulsion, positive when the rotor is dragging. The propulsive force behaves as expected; as the shaft angle increases, the propulsive force increases. Two interesting traits are of note. First, the propulsive force is sometimes negative, particularly at 860 RPM at $\mu = 0.2$, Figure 11. Second, as the rotor stalls, the propulsive force increases sharply.

An anomaly is that the 860 RPM data do not overlap the 1220 RPM data in Figures 10–12, but do in Figures 13 and 14. The data are non-dimensionalized such that it should overlap for both rotor speeds. At the lower rotor speed, errors in the dimensional forces measured result in larger non-dimensional errors than at high rotor speed. Any zero drift in the instrumentation is relatively larger with the smaller rotor forces at low advance ratio and low rotor speed. The 860 RPM $\mu = 0.15$ and $\mu = 0.20$ advance ratio data were taken during the same long run and these show the most

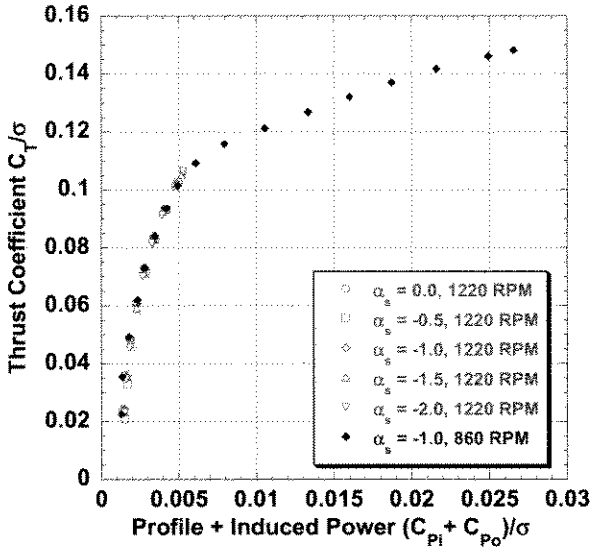

Fig. 5. Thrust vs. power at advance ratio $\mu = 0.15$, shaft angles $-2 \leq \alpha_s \leq 0$ deg, 1220 and 860 RPM.

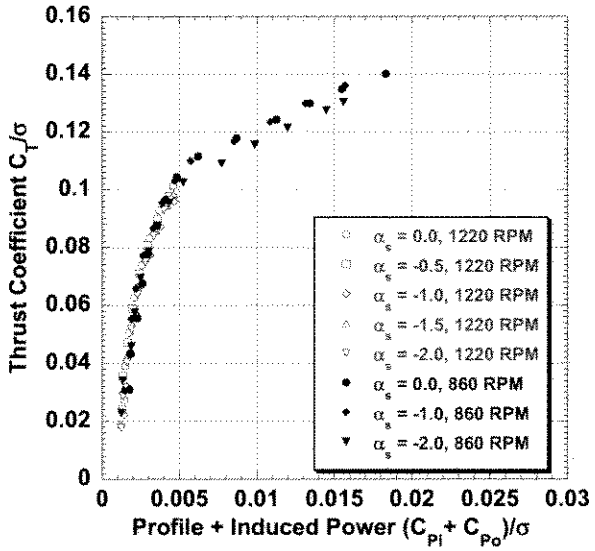

Fig. 6. Thrust vs. power at advance ratio $\mu = 0.20$, shaft angles $-2 \leq \alpha_s \leq 0$ deg, 1220 and 860 RPM.

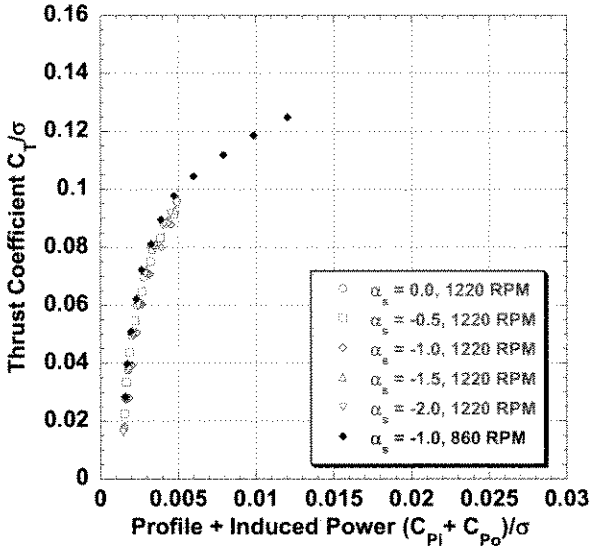

Fig. 7. Thrust vs. power at advance ratio $\mu = 0.25$, shaft angles $-2 \leq \alpha_s \leq 0$ deg, 1220 and 860 RPM.

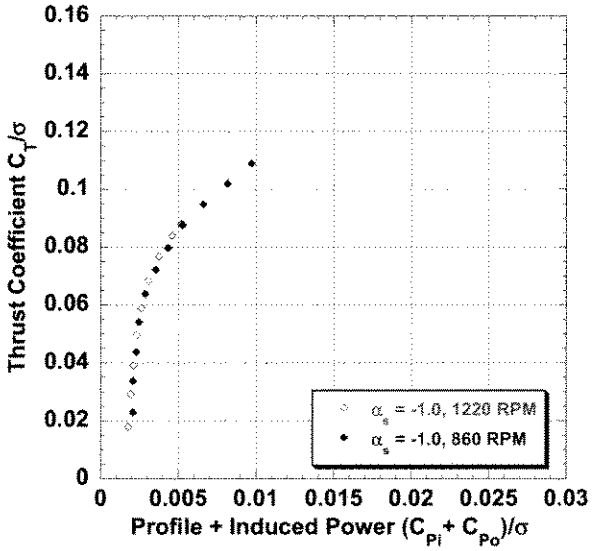

Fig. 8. Thrust vs. power at advance ratio $\mu = 0.30$, shaft angle -1 deg, 1220 and 860 RPM.

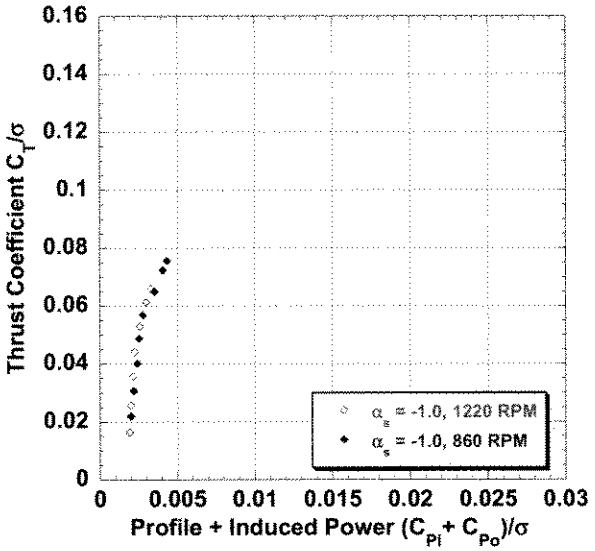

Fig. 9. Thrust vs. power at advance ratio μ = 0.35, shaft angle -1 deg, 1220 and 860 RPM.

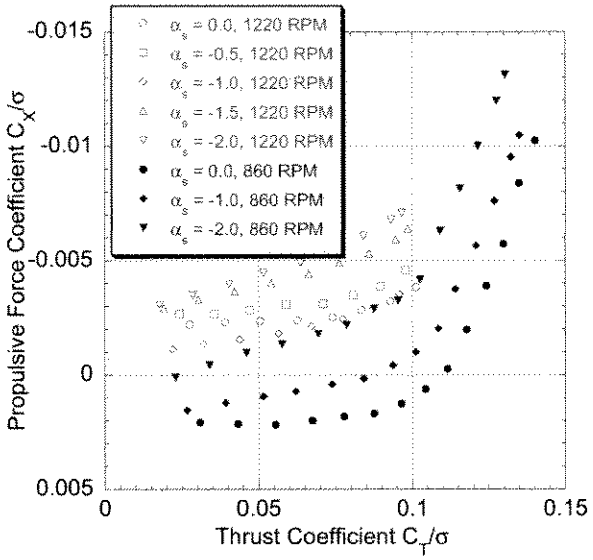

Fig. 11. Propulsive force vs. thrust at advance ratio μ = 0.20, shaft angles -2 $\leq \alpha_s \leq$ 0 deg, 1220 and 860 RPM.

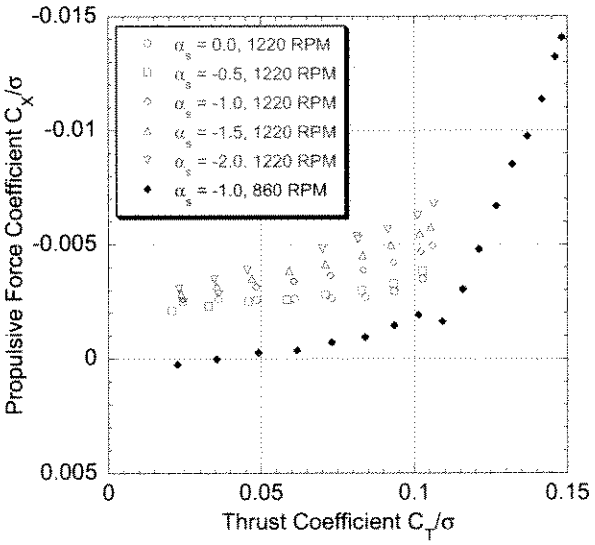

Fig. 10. Propulsive force vs. thrust at advance ratio μ = 0.15, shaft angles -2 $\leq \alpha_s \leq$ 0 deg, 1220 and 860 RPM.

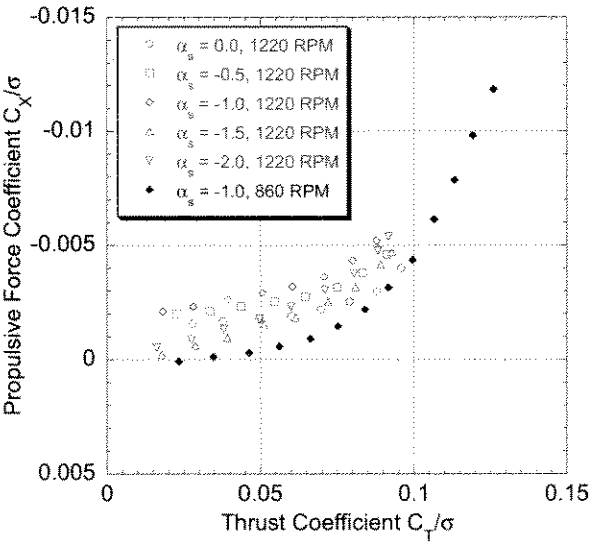

Fig. 12. Propulsive force vs. thrust at advance ratio μ = 0.25, shaft angles -2 $\leq \alpha_s \leq$ 0 deg, 1220 and 860 RPM.

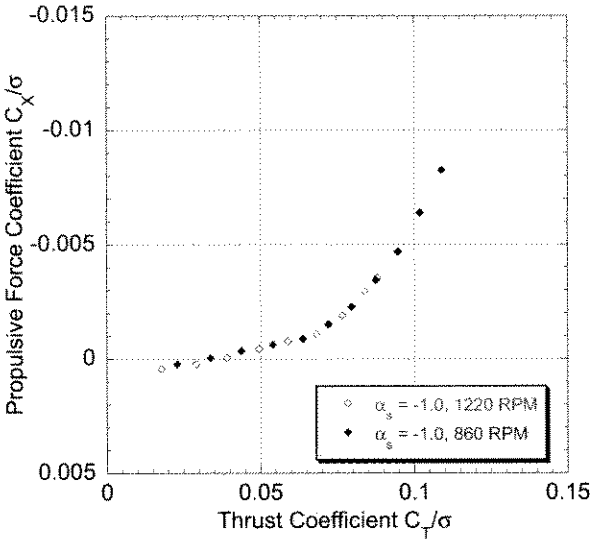

Fig. 13. Propulsive force vs. thrust at advance ratio μ = 0.30, shaft angle -1 deg, 1220 and 860 RPM.

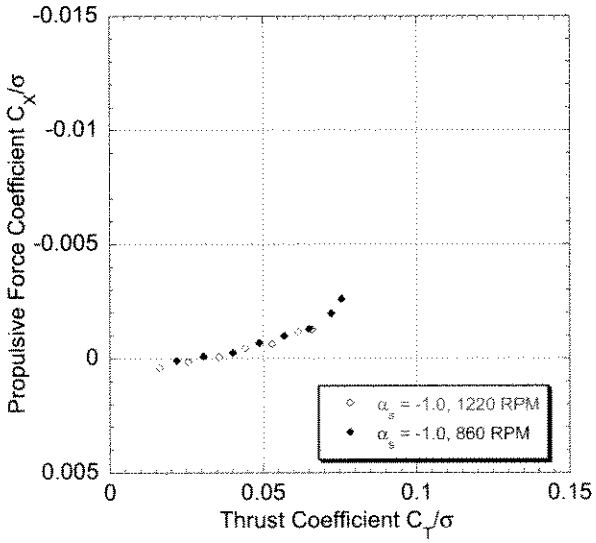

Fig. 14. Propulsive force vs thrust at advance ratio μ = 0.35, shaft angle -1 deg, 1220 and 860 RPM.

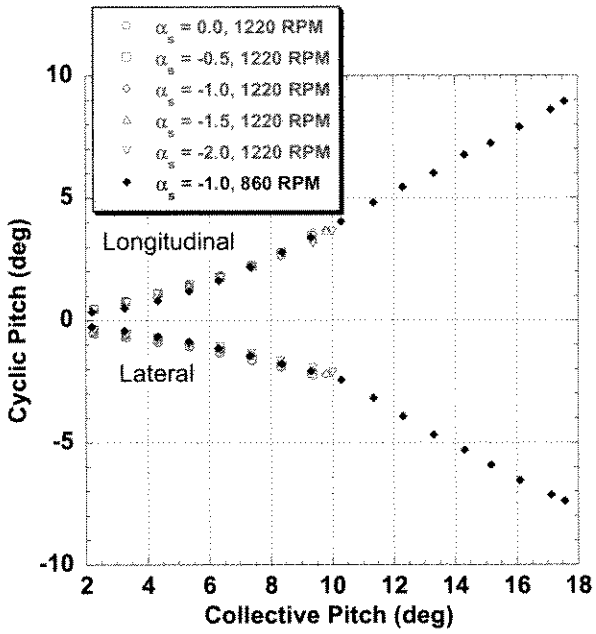

Fig. 15. Longitudinal and lateral cyclic at advance ratio μ = 0.15, shaft angles -2 $\leq \alpha_s \leq$ 0 deg, 1220 and 860 RPM.

error. A constant shift of about 0.004 would shift all four curves to be right in line with the 1220 RPM data. Likewise, the 0.25, 0.3 and 0.35 advance ratio cases were also taken during a common run. In these, the error between the 1220 RPM and 860 RPM is much smaller, so the lower advance ratio errors were most likely caused by a faulty zero measurement. It is important to note that the performance data shown in Figures 5–9 collapses to a single line using these propulsive forces. What appear to be large differences in Figures 10–12 are not large enough to visibly affect the propulsive power.

Cyclic pitch settings are shown in Figures 15–19. Longitudinal and lateral cyclic are the negative sine and cosine coefficients, respectively, measured at the pitch bearing. The controls are nearly identical at each advance ratio. This suggests that the range of shaft angles was not large enough to affect the controls. A slope change is visible, particularly in Figure 15, where stall occurs. The data on either side of this slope change are approximately linear.

To compare the controls at different advance ratios, the cyclic is plotted for a single RPM and shaft angle and several advance ratios in Figure 20. As expected, more longitudinal cyclic is required as advance ratio increases. The lateral cyclic, however, is relatively insensitive to both advance ratio and shaft angle.

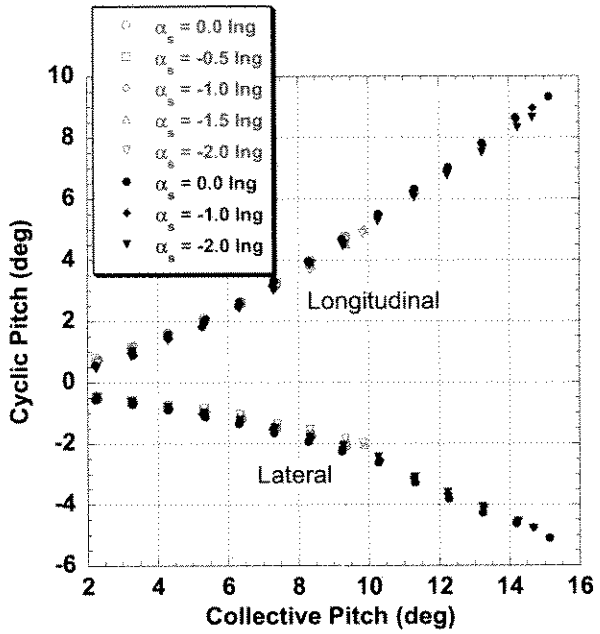

Fig. 16. Longitudinal and lateral cyclic at advance ratio μ = 0.20, shaft angles -2 $\leq \alpha_s \leq$ 0 deg, 1220 and 860 RPM.

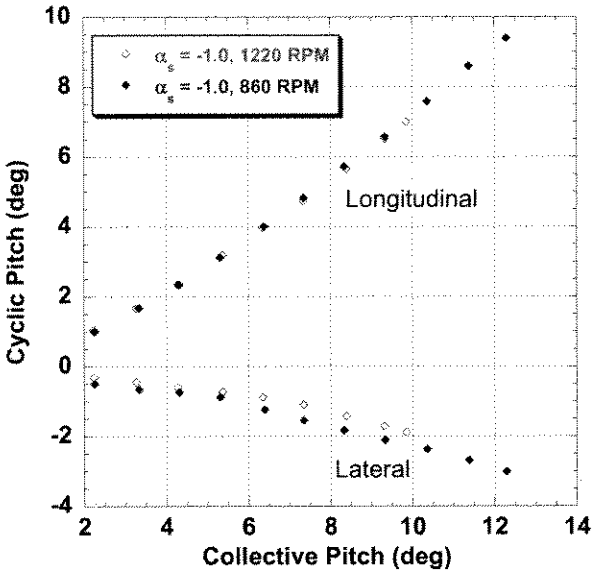

Fig. 18. Longitudinal and lateral cyclic at advance ratio μ = 0.30, shaft angle -1 deg, 1220 and 860 RPM.

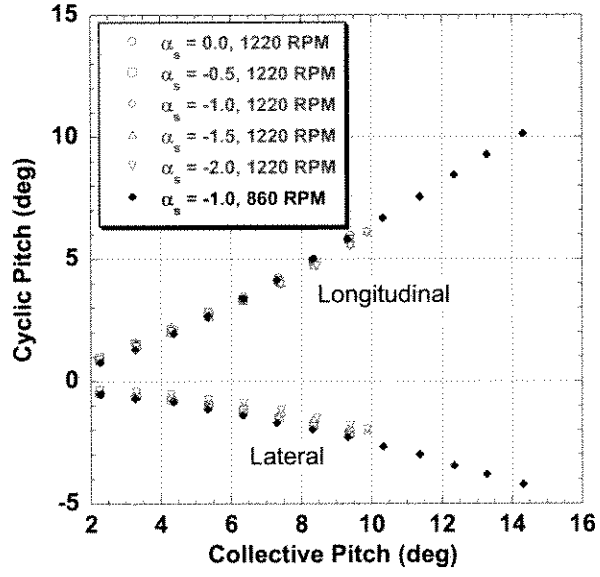

Fig. 17. Longitudinal and lateral cyclic at advance ratio μ = 0.25, shaft angles -2 $\leq \alpha_s \leq$ 0 deg, 1220 and 860 RPM.

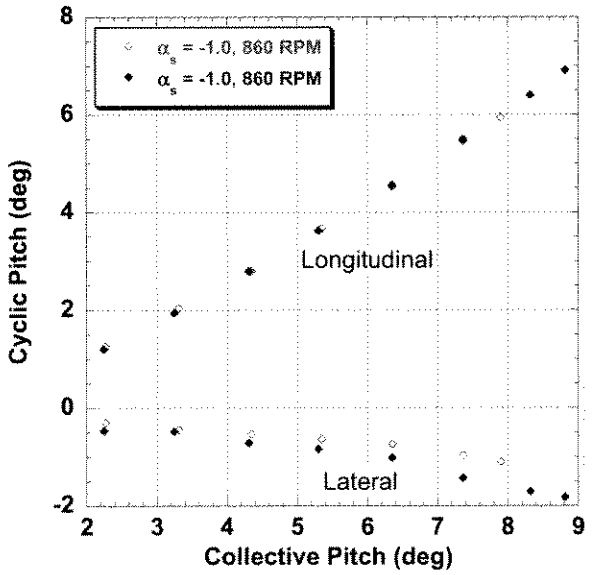

Fig. 19. Longitudinal and lateral cyclic at advance ratio μ = 0.35, shaft angle -1 deg, 1220 and 860 RPM.

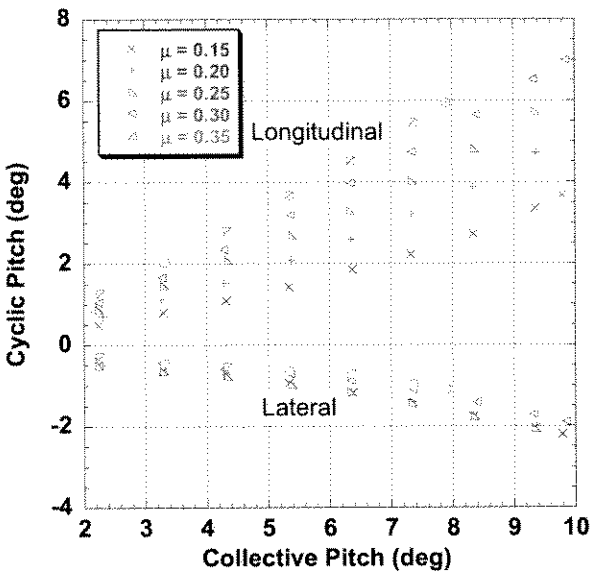

Fig. 20. Longitudinal and lateral cyclic at 1220 RPM, shaft angle -1 deg, $0.15 \leq \mu \leq 0.35$.

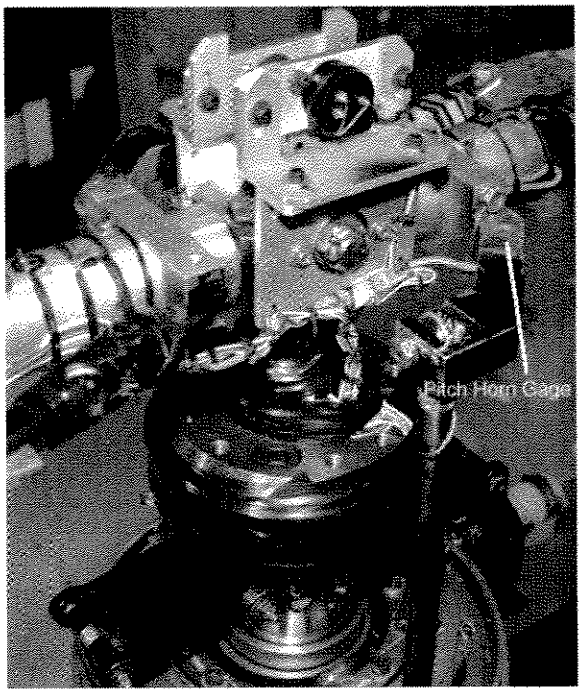

Fig. 21. Photo of rotor hub showing pitch link and pitch horn with instrumentation.

Loads Data

Redundant measurements of blade torsional loads were recorded. A shear strain gage on the instrumented blade (see Figures 2 and 3) and strain gages on each of the pitch horns (see Figure 21) recorded separate measurements of the blade torsional loads. The pitch horn loads were calibrated to output blade root torsion directly rather than output the bending moment in the pitch horn. Note that the terms "pitch horn loads" and "pitch link loads" are used interchangeably here, even though the load is physically measured only on the pitch horn.

Time history data from these sensors were processed to show the change in loads as the rotor began to stall. The raw time histories contain about 56 revolutions of data at 1024 samples per revolution. A digital filter was used to extract the vibratory pitch link loads. Only low frequency harmonic data are of interest, so other frequencies were removed with the filter. Two different techniques were used.

In the first method, the data were averaged to produce a single average revolution with 1024 data points. The averaging removes all frequencies that are not harmonics of the rotor speed. An FFT was performed on the data and the mean, 1/rev, and > 15/rev spectral lines were removed so that only harmonics from 2–15 were present. The signal was then transformed back into a time history using a reverse FFT. The half peak-to-peak magnitudes were obtained from this time history.

In the second method, the half peak-to-peak was calculated over many revolutions at once. First the data were truncated to 32 revs (32768 samples) to accommodate the FFT algorithm, then several filters were applied. The first filtering done to the data was the removal of a persistent 7.6/rev signal. 7.6/rev corresponds to a 3/rev motor frequency. The motors used three phase power, so the signal is thought to be electrical interference. The forward-reverse FFT procedure discussed above was used to obtain notch and band-pass filters. The notch filter removed frequencies between 7.4/rev and 7.8/rev from the data. The band pass filter removed everything except content between 1.5/rev to 15/rev.

There are important differences between this signal and the averaged signal discussed above. First, it is 32 revs long rather than one. Second, and more importantly, non-integer harmonics were retained. For a wind tunnel test, all data should be periodic with the rotor speed, so the amount of non-integer harmonic content is a measure of the data quality.

The half peak-to-peak data for averaged rotor revolutions are shown in Figures 22–26. The moments are nondimensionalized by $\rho A V_T^2 R$ so that the 860 RPM and 1220 RPM data can be shown on the same plot. The pitch link loads are larger than the blade torsion loads in every instance. Additionally, the pitch link loads are different from each other. In theory, the pitch link loads should be the same for the two blades if the blades are identical.

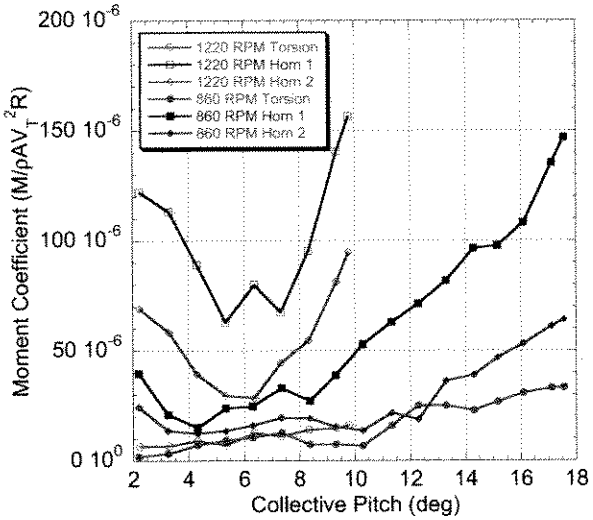

Fig. 22. Half peak-to-peak torsion loads measured by the blade torsion strain gage and the pitch horn strain gages μ = 0.15, shaft angle -1.0 deg, 1220 and 860 RPM.

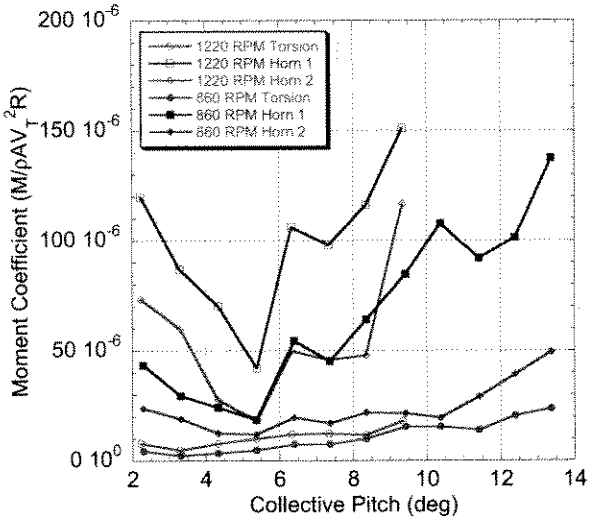

Fig. 24. Half peak-to-peak torsion loads measured by the blade torsion strain gage and the pitch horn strain gages μ = 0.25, shaft angle -1.0 deg, 1220 and 860 RPM.

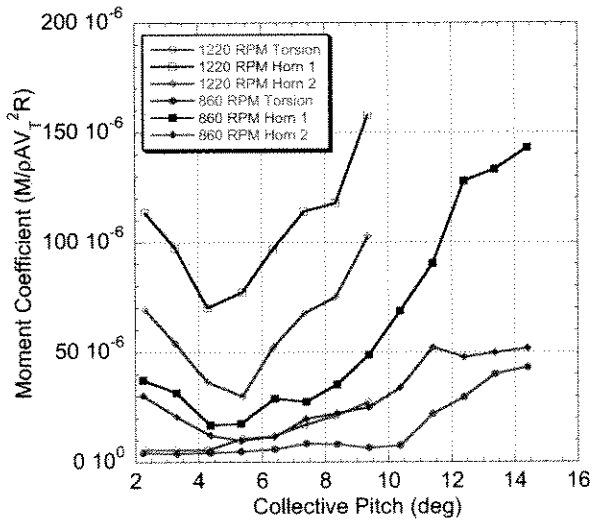

Fig. 23. Half peak-to-peak torsion loads measured by the blade torsion strain gage and the pitch horn strain gages μ = 0.20, shaft angle -1.0 deg, 1220 and 860 RPM.

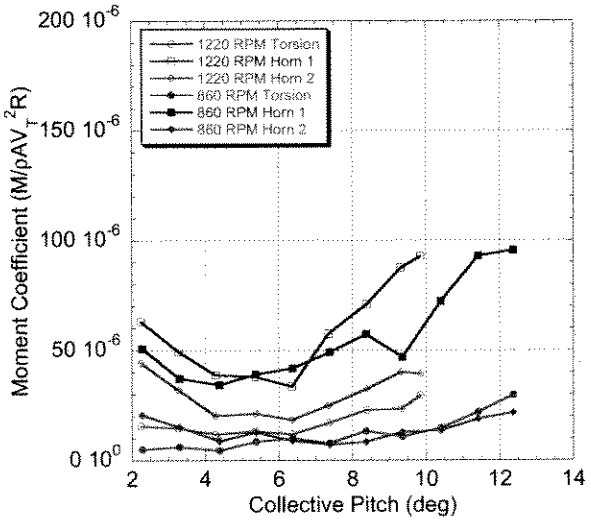

Fig. 25. Half peak-to-peak torsion loads measured by the blade torsion strain gage and the pitch horn strain gages μ = 0.30, shaft angle -1.0 deg, 1220 and 860 RPM

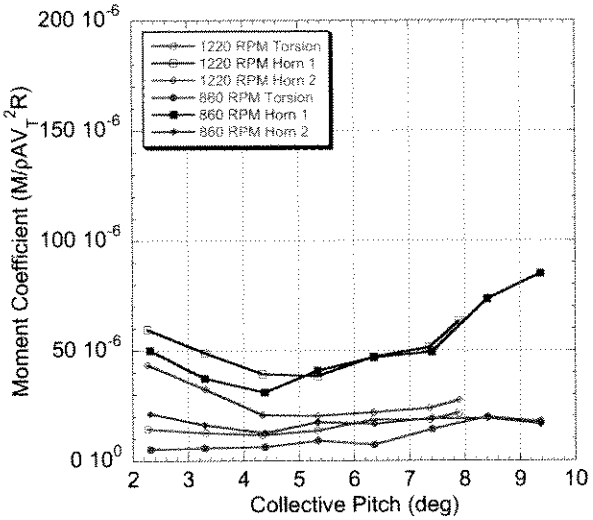

Fig. 26. Half peak-to-peak torsion loads measured by the blade torsion strain gage and the pitch horn strain gages μ = 0.35, shaft angle -1.0 deg, 1220 and 860 RPM.

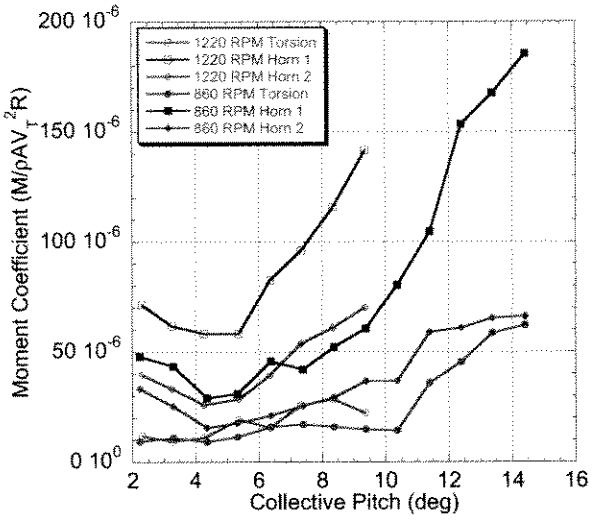

Fig. 27. Half peak-to-peak torsion loads measured by the blade torsion strain gage and the pitch horn strain gages μ = 0.20, shaft angle -1.0 deg, 1220 and 860 RPM (data not averaged).

As an example, half peak-to-peak loads for unaveraged data (the second data reduction method described above) at $\alpha_s = -1.0$ deg and $\mu = 0.20$ are shown in Figure 27. Comparing Figure 27 to Figure 23, it is difficult to make a sweeping statement. The raw data is the same, so the only difference between the two is the averaging/filtering method. From these specific plots, the greatest error is about 50%, in the 1220 RPM horn 1 and 860 RPM torsion. For the other results (not shown), differences ranged from small to 100%, indicating that there is enough noise and nonharmonic content in the loads measurements to significantly impact half peak-to-peak measurements.

To investigate further, raw data was examined more closely by comparing the three measurements at the same condition. Figure 28 shows time histories of the torsion loads measured by both of the pitch horn gages and the blade torsion gage at the highest thrust condition for 860 RPM, $\mu = 0.15$, $\alpha_s = -1.0$. On each plot in the figure, the averaged data are plotted in black, and five individual revolutions are superimposed in light gray behind. This allows comparison of the averaged data with raw data and the averaged data from different measurements with each other.

The scales of the two pitch horn traces are different, but the signal is similar. Pitch horn 1 has more higher harmonic content, but the basic shape matches between the two. The measured calibration coefficients between the two blades were nearly identical and for a static torsion load, the data system recorded the same moment for both blades. So the scale difference is assumed to be from a blade to blade difference. The most likely source of the error is the 0.10 inch difference in the chordwise cg between the blades, which translates to a 2.5% chord difference.

The shape of the two pitch horn plots are similar, but this is not so for the blade torsion gage, shown in the bottom plot. This time history is not only a much smaller scale, but is very different qualitatively. This suggests that either there were significant externally applied torsion loads on the blade inboard of the torsion gage, or that the placement of the torsion gage on the surface of the fiberglass skin does not provide accurate measurements of the loads carried in the spar. The blade inboard of the torsion gage is short and operating at low dynamic pressure, but does go in and out of the reverse flow region, so either is possible.

To assess if the differences in the half peak-to-peak loads were consistent over a range of conditions, the loads were plotted against each other for a range of advance ratios. Pitch horn 1 was used as the baseline since it had the commonality of being on the same blade as the blade torsion gage and was the same type of measurement as pitch horn 2. Figure 29 shows the latter two measurements plotted against the former. All five advance ratios are represented for 1220 RPM and -1.0 deg shaft angle. If the measurements were all the same, the points would lie along a 45 deg line. The plot instead shows that the pitch horn 2 points lie along a line with a slope of about 1/2 and the torsion measurements have a slope near zero. This indicates that there is a factor of 2 difference between the two pitch horn measurements and that the measured blade torsion does not increase with either thrust or advance ratio.

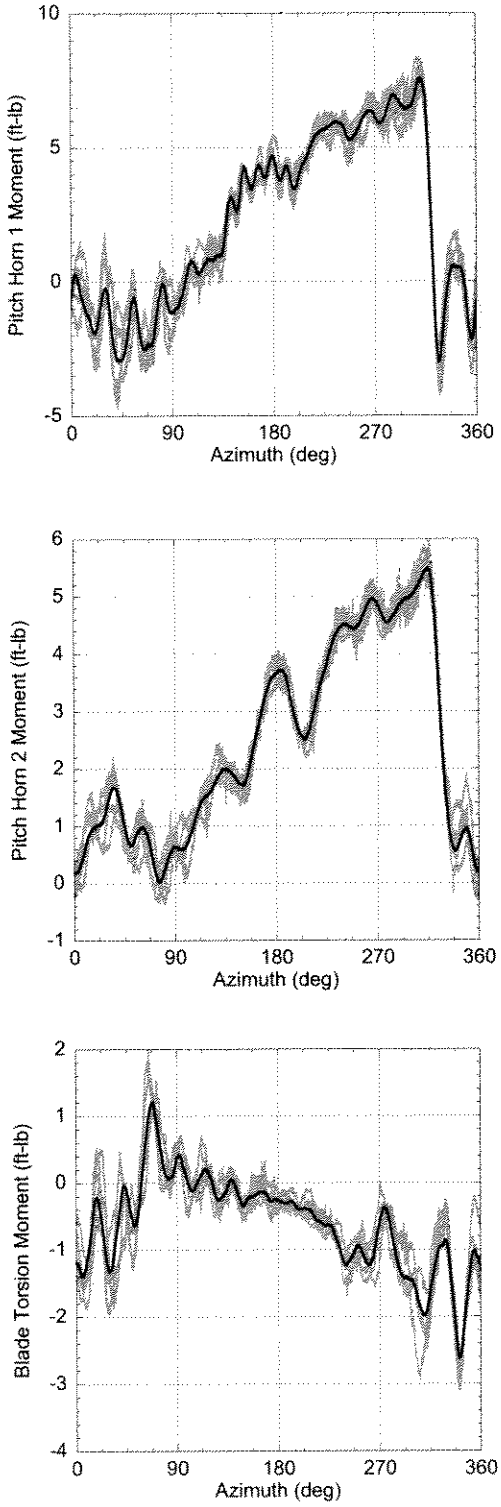

Fig. 28. Time histories of blade torsion loads compared to the average for the two pitch horn gages and the blade torsion gage, μ = 0.15, 860 RPM, α_s = -1.0, C_T/σ= 0.148.

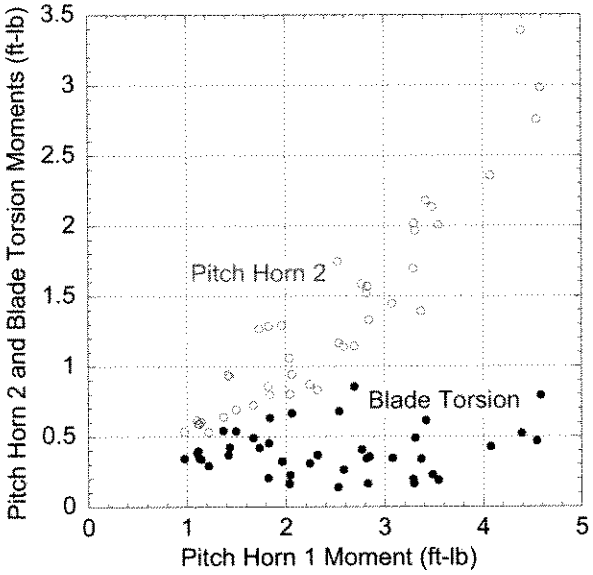

Fig. 29. Blade torsion of pitch horn 2 and torsion vs. pitch horn 1. 0.15 $\leq \mu \leq$ 0.35, α_s = -1.0, 1220 RPM.

Although the two pitch horn measurements differ by a factor of about 2, the measurements are qualitatively similar and the difference is consistent. While not as desirable as identical measurements, the data have some value. The blade torsion measurements, however, do not appear to match either of the pitch horn measurements and do not increase with advance ratio or thrust. The data are therefore not used for correlation.

Comparison with Historical Tests

Similar data obtained by McHugh and in the UH-60 Airloads Program were compared by Yeo (Ref. 8). The data were surprisingly similar between the two tests considering the differences in the rotors. The rotors had different twist, chord, solidity, and number of blades, but the trends of thrust with power were very similar. Data from the current test were compared with these two previous tests for those flight conditions which overlapped for all three tests.

The comparisons of thrust and power are shown for $\mu = 0.2$ in Figure 30 and for $\mu = 0.3$ in Figure 31. Several observations are made. For a given power coefficient, the rotor in the current test provides less thrust for all of the data shown. This is to be expected considering that an NACA 0012 airfoil was used in the current test, while airfoils from more modern production aircraft were used for the other two tests. The second observation is that the amount of thrust at a given power increases with the size of the rotor used in the test. The rotor in the present test is the smallest rotor, followed by McHugh's scaled CH-47 rotor,

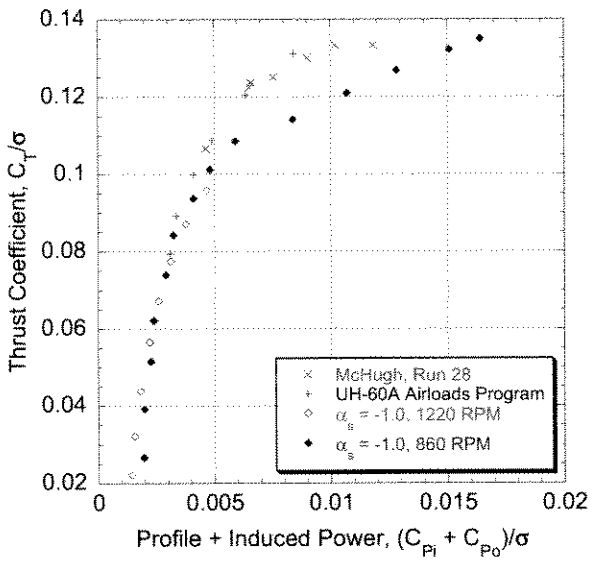

Fig. 30. Comparison of thrust and power data reported in ref. 8 with data from current test at 860 and 1220 RPM, $\mu = 0.2$.

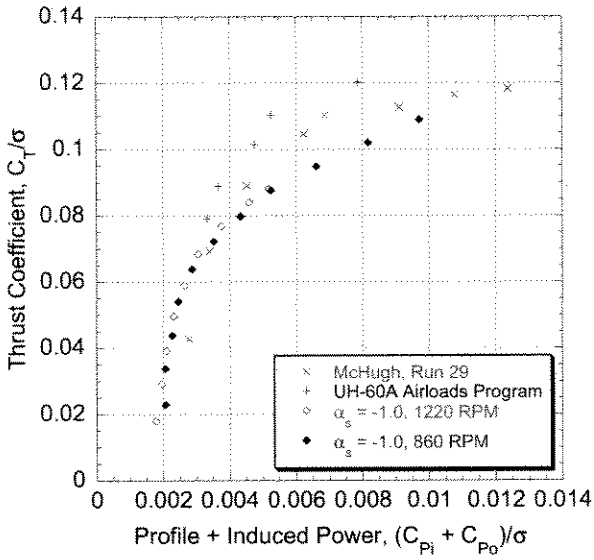

Fig. 31. Comparison of thrust and power data reported in ref. 8 with data from current test at 860 and 1220 RPM, $\mu = 0.3$.

and the UH-60 data are from a full-scale flight test. This could be a Reynolds number effect.

Another observation is in the stall character, particularly at $\mu = 0.2$. For the historical tests, the post-stall thrust falls off more quickly than for the current test. At both advance ratios, the current data look approximately linear post stall. This is the case for Figures 5–8 as well. In contrast, the thrust slope for the historical data continue to decrease such that the slope between two highest thrust points is nearly zero, indicating thrust reversal is imminent.

The rotor in the current investigation was significantly different from both of the previous two in several important aspects. First, it was untwisted. Second, the present rotor was teetering, so flapping moments due to coning were not relieved as they would be in an articulated rotor. Both the UH-60 and CH-47 rotors are articulated. Third, the present rotor is a symmetric NACA 0012 airfoil whereas the other rotors used airfoils developed at Boeing and Sikorsky that were specifically designed for helicopters. Finally, the trim conditions were different. For the McHugh data, the rotor was trimmed to a constant propulsive force, and this propulsive force was maintained while thrust increased.

This propulsive force issue should not be a factor in the comparison for several reasons, however. The most important of which is that the data from the three tests are being presented with propulsive power removed. For large propulsive forces, there would be an effect on thrust, but the difference in propulsive force between tests should be moot for small propulsive forces here. Additionally, the data for the current test collapsed nearly to a single line at a given advance ratio, so any of the shaft angle conditions (corresponding to differing propulsive power) could be used interchangeably for comparison. Moreover, as discussed previously, the primary flight condition of $\mu = 0.2$, α_s of -1.0 deg was chosen to approximately match the propulsive force coefficient $X/(qd^2\sigma)$ of 0.05 from the McHugh data at a thrust coefficient $C_T/\sigma = 0.08$.

CAMRAD II Correlation

The rotor performance was also correlated with the comprehensive analysis CAMRAD II (Ref. 12). A CAMRAD II model of the rotor was developed initially for pre-test safety predictions and later refined for correlation with the test data. The model was compared with nonrotating blade frequencies and later with the performance data collected during the test.

The model was an elastic blade model with four elements for each blade. The properties were calculated from drawings of the spar and attachment hardware. The blade had a constant chord and constant thickness. Therefore, knowing the dimensions of the spar and the spruce trailing edge, the dimensions of the balsa filler could be calculated. The properties were numerically integrated in a spreadsheet to obtain the blade properties, presented in Table 2.

To verify the blade properties used in CAMRAD, a rap test was conducted on a cantilevered blade. The blade was hard mounted to the floor, not on the hub. The frequencies

Table 2. Distributed properties for CAMRAD II blade model

Radial Station, fraction R	0.0	0.185	0.2031	0.2032	0.2517	0.4181	0.7091	1.0
Mass, slug/ft	0.081	0.081	0.037	0.051	0.047	0.022	0.016	0.0156
I_θ, 10^{-6} slug-ft	593	593	478	488	312	46.0	44.3	44.3
I_P, 10^{-6} slug-ft	590	590	475	479	303	42.5	42.2	42.2
X_{cg}, fraction R	0.0	0.0118	0.00504	0.0169	0.0126	-0.00174	-0.00240	-0.00240
X_{tc}, fraction R	0.0	0.0130	0.0186	0.0167	0.0122	-0.00683	-0.00962	-0.00962
EI_{LAG}, 10^3 lb-ft^2	240	117	89.0	83.6	58.8	5.90	4.62	4.62
EI_{FLAP}, 10^3 lb-ft^2	8.00	3.95	0.401	1.26	1.24	0.496	0.292	0.292
GJ, 10^3 lb-ft^2	50.0	45.9	33.9	32.0	22.5	1.57	0.857	0.857
EA, 10^6 lb	46	22.2	10.0	13.7	12.5	5.00	3.43	3.43
K_P, fraction R	0.0249	0.0249	0.0332	0.0283	0.0236	0.0125	0.0147	0.01467
K_T, fraction R	0.0249	0.0249	0.0332	0.0283	0.0236	0.0125	0.0147	0.01467

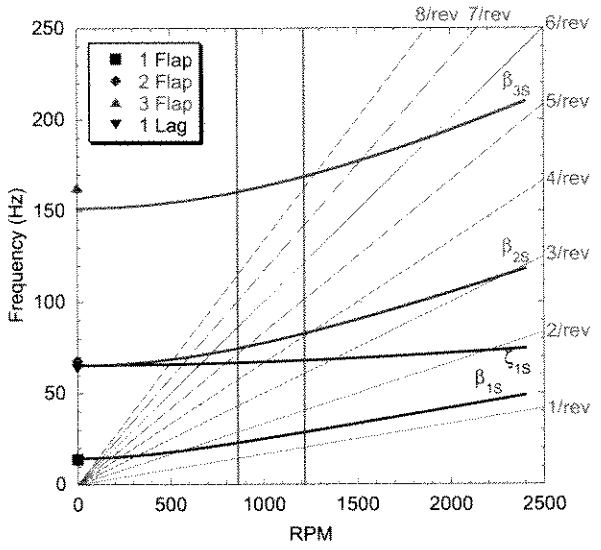

Fig. 32. Rap test frequencies of isolated blade compared with fan plot of symmetric modes calculated in CAMRAD II.

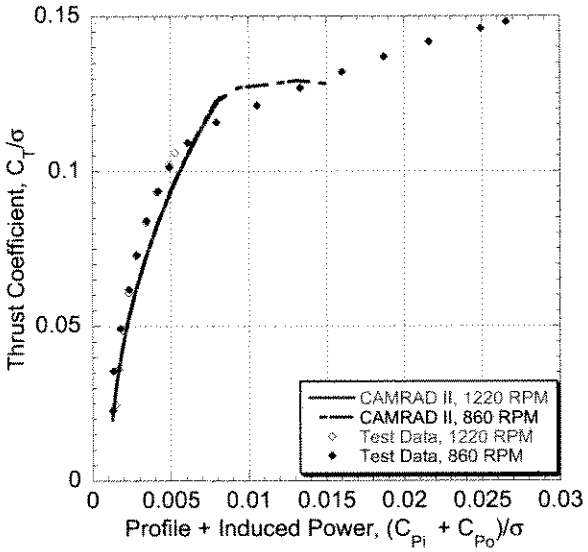

Fig. 33. Calculated thrust vs. power compared with test data at advance ratio μ = 0.15, -1 deg shaft angle.

should be the same as the symmetric modes calculated in CAMRAD II. A fan plot with the rap test frequencies included is shown in Figure 32. The bending modes agree well with the rap test results. No torsion mode was found experimentally below 200 Hz, consistent with a very high frequency predicted in CAMRAD II.

In order to capture the detailed aerodynamics of the model, 20 aerodynamic panels and a free wake model were used. A dynamic stall model was not used and no correction was made for the rotor being in a wind tunnel. The rotor trim was calculated to match the test procedure. The shaft angle, RPM, and collective pitch were fixed, and the trim procedure calculated the lateral and longitudinal cyclic pitch required to trim the rotor to zero flapping.

Thrust and power predictions from CAMRAD II are compared with the test data in Figures 33–37 for a shaft angle of -1.0 deg. The predictions agree quite well with the test data, with some notable exceptions. At μ of 0.15 and 0.2, the stall predicted by CAMRAD is more abrupt and severe. The rotor thrust reaches a maximum and further increases in collective do not increase thrust further. The sharply defined stall smooths out as advance ratio increases. The prediction tracks the test data very closely for advance ratios of 0.25 and higher.

Conclusions

A test was conducted in the 7- by 10-Foot Wind Tunnel at Ames Research Center to measure rotor thrust entering

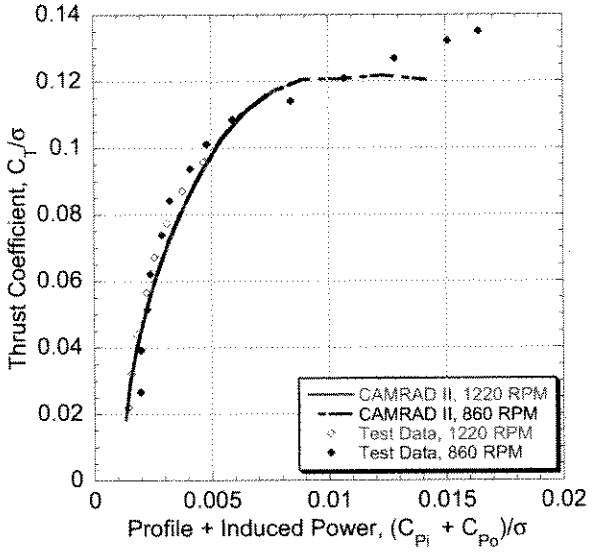

Fig. 34. Calculated thrust vs. power compared with test data at advance ratio μ = 0.20, -1 deg shaft angle.

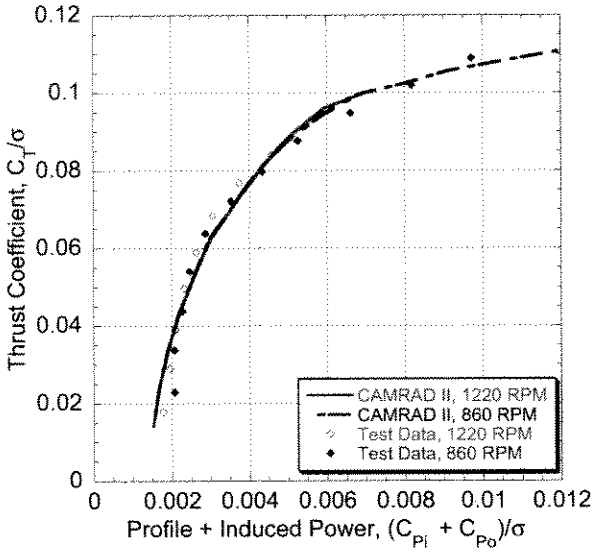

Fig. 36. Calculated thrust vs. power compared with test data at advance ratio μ = 0.30, -1 deg shaft angle.

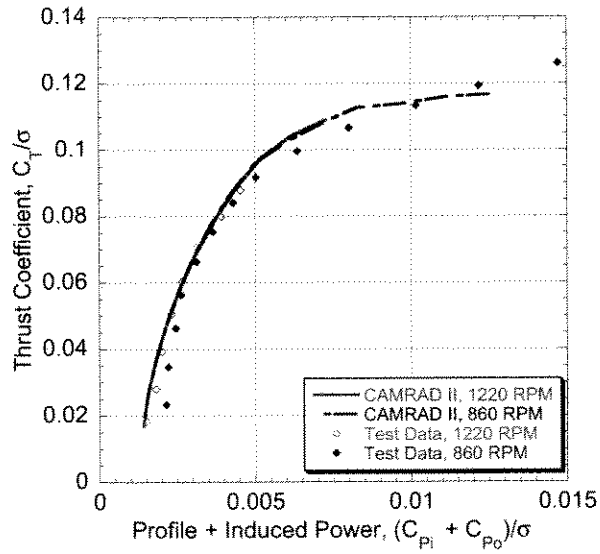

Fig. 35. Calculated thrust vs. power compared with test data at advance ratio μ = 0.25, -1 deg shaft angle.

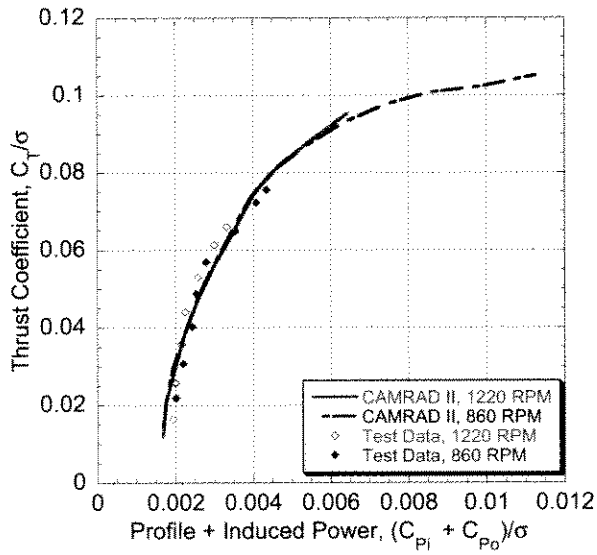

Fig. 37. Calculated thrust vs. power compared with test data at advance ratio μ = 0.35, -1 deg shaft angle.

stall. The data obtained were limited in terms of tip speed and maximum thrust by the rotor balance and blade loads. In any subsequent test, a larger capacity balance and an articulated rotor should be used. Nonetheless, thrust levels as high as $C_T/\sigma = 0.146$ were achieved during the test. Specific conclusions follow.

1. Rotor thrust and power measurements were high quality and repeatable with changes in shaft angle and rotor speed. Propulsive force results showed some anomalies, but these were limited to one series of runs that most likely contained a bad zero. Propulsive force anomalies were not of sufficient magnitude to affect the calculation of profile plus induced power.

2. Noise in the loads measurements caused half peak-to-peak loads in the raw data to be up to 100% greater than those in the averaged data. Most of the differences were 50% or less.

3. The pitch link loads data were similar for the two pitch horn measurements. A factor of 2 difference in scale was observed, but the qualitative character of the data was consistent between the two sensors. The blade torsion gage measurements were completely different in character and scale from the pitch horn data and did not increase in magnitude with either advance ratio or thrust.

4. The rotor in the current test produces less thrust at a given power than the rotors in the McHugh test and the UH-60 Airloads Program. Possible contributors are selection of airfoil, blade twist, and hub type.

5. CAMRAD II calculations with a static stall model compare well with the test data at advance ratios of 0.25 and above, reasonably well for advance ratios of 0.15 and 0.2.

Acknowledgments

The authors would like to thank the US Army Aeroflightdynamics Directorate staff at the 7- by 10-Foot Wind Tunnel for their hard work in executing this test in a short period of time.

References

[1]Leishman, J. G. and Beddoes, T. S., "A Semi-Empirical Model for Dynamic Stall," *Journal of the American Helicopter Society*, Vol. 34, (3), July 1989.

[2]Petot, D., "Differential Equation Modeling of Dynamic Stall," Technical Report 1989-5, La Recherche Aerospatiale, (Corrections dated October 1990), 1989.

[3]Truong, V. K., "A 2-D Dynamic Stall Model Based on Hopf Bifurcation," Proceedings of the Nineteenth European Rotorcraft Forum, Marseilles, France, September 1998.

[4]Nguyen, K. and Johnson, W., "Evaluation of Dynamic Stall Models with UH-60A Airloads Flight Test Data," Proceedings of the American Helicopter Society 54th Annual Forum, Washington, DC, May 1998.

[5]McHugh, F. J., Clark, R., and Solomon, M., "Wind Tunnel Investigation of Rotor Lift and Propulsive Force at High Speed—Data Analysis," NASA CR 145217-1, Langley Research Center, October 1977.

[6]McHugh, F. J., Clark, R., and Solomon, M., "Wind Tunnel Investigation of Rotor Lift and Propulsive Force at High Speed—Test Data Appendix," NASA CR 145217-2, Langley Research Center, October 1977.

[7]McHugh, F. J., "What are the Lift and Propulsive Force Limits at High Speed for the Conventional Rotor?" Paper No. 78-2, Proceedings of the American Helicopter Society 34th Annual Forum, May 1978.

[8]Yeo, H., "Calculation of Rotor Performance and Loads Under Stalled Conditions," Proceedings of the American Helicopter Society 59th Annual Forum, Phoenix, Arizona, May 2003.

[9]Kufeld, R. M., Balough, D. L., Cross, J. L., Studebaker, K. F., Jennison, C. D., and Bousman, W. G., "Flight Testing the UH-60A Airolads Aircraft," Proceedings of the American Helicopter Society 51st Annual Forum, Washington, DC, May 1994.

[10]Johnson, W., *Helicopter Theory*, Dover Publications, Inc., 1980.

[11]McAlister, K. W., Tung, C., Sharpe, D. L., Huang, S., and Hendley, E. M., "Preliminary Study of a Model Rotor in Descent," NASA TM 2000-208785, Ames Research Center, November 2000.

[12]Johnson, W., "Rotorcraft Aeromechanics Applications of a Comprehensive Analysis," Presented at Heli Japan 98: AHS International Meeting on Advanced Rotorcraft Technology and Disaster Relief, Japan, April 1998.